Surface−Atom Transfer Radical Polymerization from Silica Nanoparticles with Controlled Colloidal Stability

Abdeslam El Harrak, Géraldine Carrot,* Julian Oberdisse, Christophe Eychenne-Baron,† and François Boué

Laboratoire Léon Brillouin, CEA/CNRS, Bâtiment 563, CEA/Saclay, 91191 Gif-sur-Yvette, France

Received December 19, 2003; Revised Manuscript Received June 2, 2004

ABSTRACT: Polymer chains are grafted from silica beads (colloidal sol in dimethylacetamide) by atom transfer radical polymerization (ATRP). The method consists of grafting first the initiator molecules on the silica surface ("grafting from" method), in two steps. First, thiol-functionalization of the surface was achieved via silanization with a mercaptopropyl triethoxysilane. Second, we performed an overgrafting of the surface by reacting the thiol with 2-bromoisobutyryl bromide to generate the halogen-functional ATRP initiator. From that, the polymerization of styrene was conducted. Control of both the molecular weight and the density of grafted chains can be achieved by this method. The other originality of this work is that we keep the nanoparticles in solution at each stage of the procedure (even during the purification steps), as this is the only way to avoid irreversible aggregation. The state of dispersion of the grafted nanoparticles is followed by small-angle neutron scattering. Characterizations such as gel permeation chromatography, ^{29}Si CP/MAS NMR, elemental analysis, infrared spectroscopy, and thermogravimetric analysis are conducted to confirm the success of the grafting reaction.

Introduction

Polymeric materials generally show improved mechanical and thermal properties after addition of inorganic fillers such as silica nanoparticles.[1] The main challenge is then to control the level of interparticle aggregation. The attraction between the nanoparticles is enhanced by the fact that the polymer matrix is generally hydrophobic, while the surface of silica is hydrophilic. To have well-separated nanoparticles throughout the synthesis, we started from colloidal solutions. There, the two general types of stabilization to prevent aggregation are charge and steric stabilization.[2] Electrostatic stabilization is based on repulsive electrostatic forces between charged surfaces. In a previous study, some of us have taken advantages of this by mixing silica nanoparticles with polymer latex beads with a polystyrene/poly(*n*-butylacrylate) core and a charged poly(acrylic acid) shell.[3] Controlling the charge via the pH has shown that improvement of the mechanical properties is strongly linked to the state of aggregation of nanoparticles in the polymer matrix.

In the present work, we used the other route, steric stabilization, to improve the control of nanoparticles aggregation by grafting long polymer chains. However, to shift from one to another type of stabilization, one must overcome the inherent difficulties of changing the hydrophobic/hydrophilic balance of the surface in the initial colloidal dispersion. The colloidal stability requires a good balance between the decrease in entropy of particles due to the increase in mass brought by the grafted chains, and an increase in osmotic pressure.[4] Such stability can be kept when transferring the grafted particles in a polymer matrix. At this stage, a second advantage of grafting polymer chains is to improve the compatibility of the matrix chains with the particle surface.

* Corresponding author. Phone: (00-33)-1 69 08 60 37. E-mail: carrot@llb.saclay.cea.fr.

† Present address: Rhodia, Centre de Recherche Aubervilliers, 52, rue de la Haie Coq, F-93308 Aubervilliers Cedex, France.

The functionalization of nanoparticles with polymers has been performed via the "grafting from" method. This approach reported for the first time by Prucker and Rühe consists of grafting the initiator molecules followed by polymerization.[5] The main advantage of this method over the "grafting onto" one is the control of the grafting density. Since this work, a large number of papers have reported improvement of this grafting technique using controlled/living radical polymerization, atom transfer radical polymerization (ATRP)[6] to control the molecular weight of the grafted polymer chains from flat surfaces[7] and, more recently, from particles.[8]

In particular, Patten has reported ATRP from silica particles.[8a] He shows that polymerization of styrene and methyl methacrylate from 75-nm particles can be successfully performed with a high degree of control during the polymerization despite a deviation from theoretical molecular weights. However, when the particles are larger (300 nm), the polymerization does not exhibit molecular weight control, unless a small amount of free initiator is added to induce the polymerization.

Our approach consisted of using colloidal silica nanoparticles (10 nm in diameter) dispersed in an organic solvent (dimethylacetamide) and of conducting a multistep reaction where particle properties were modified gradually. For each step, we verified that the nanoparticles suspension was still stable. Parallel to this work, Matyjaszewski et al. report a very well-presented and detailed kinetic study of ATRP from similar nanoparticles (20 nm diameter in organic solvent).[8g] They show that polymerization can be performed with a high degree of control, with addition of $Cu(II)Br_2$ as the deactivating transition-metal species. Nevertheless, nanoparticles have not been maintained in solution but redispersed after being dried, although it is well known that drying and redispersion may induce a risk of irreversible aggregation.

In the present work, we have focused on two specific points. First, the self-assembly of the initiator was done in two steps, that is, grafting a commercial mercapto-

10.1021/ma035959w CCC: $27.50
Published on Web 07/29/2004

silane followed by the esterification of the thiol group. We expected this method to ensure a better control of the grafting. A similar technique has been used in the vapor phase for the functionalization of planar surfaces and was shown to lead to a more uniform layer as compared to the direct grafting of ((2-bromo-2-methyl)-propionyloxy)hexyltriethoxysilane).[7h] Second, the nanoparticles were kept in the same solvent throughout the process (functionalization and polymerization). We have done a systematic characterization of the nanoparticles dispersion at the different stages of the reaction and after polymerization using small-angle neutron scattering (SANS), showing that particles do not aggregate during the process.

Experimental Section

Materials. Styrene was purified by distillation from calcium hydride. Mercaptopropyl triethoxysilane (MPTS) was purchased from ABCR. Anhydrous pyridine (99.8%), (dimethylamino)pyridine (DMAP), dimethylacetamide (DMAc), 2-bromoisobutyrate bromide, *N*,*N*,*N*′,*N*′,*N*″-pentamethyldiethylenetriamine (PMDETA), and copper(I) bromide (99.999%, stored under nitrogen) were used as received from Aldrich. Silica nanoparticles in a 20 wt % sol in dimethylacetamide were kindly provided by Nissan (DMAC-ST) and used as received. SANS from dilute solutions is described by a log-normal distribution with an effective mean diameter of 14 nm, and hence a specific area of 190 m^2/g.

Characterization. Number average molecular weights (M_n), weight average molecular weight (M_w), and molecular weight distribution (M_w/M_n) were determined using gel permeation chromatography (GPC) in THF at 30 °C with a flow rate of 1 mL min^{-1}. Two 7.5 mm diameter × 300 mm Polymer Labs 5 μm particle diameter mixed-D PLgel columns were connected in line to a Shimadzu LC-10AD pump, a degasser (Erma, ERC-3312), a Shimadzu RID-6A differential refractive index (DRI) detector, and a PD 2000 (Precision Detectors, Inc.) two-angle light scattering (TALLS) detector. The static measurements were done both at 15° and 90° and were simultaneously coupled to a dynamic light scattering analysis.

^{1}H nuclear magnetic resonance spectroscopy was done on a Bruker AC200 FT-NMR spectrometer using the solvent peak as a reference. Solid-state ^{29}Si CP/MAS NMR spectra were obtained from an Avance 300 instrument (with a 4 mm probe at the magic angle rotation of 4 Hz). Quantitative measurements were performed from simple impulsion (90° pulse and 120 s for recycling time). Nonquantitative measurements were obtained from cross-linked polarization (contact time: 2 ms).

Thermogravimetric analysis (TGA) was performed on a TA instrument Q50, at a scan rate of 20 °C min^{-1}, up to 800 °C under air. Differential scanning calorimetry (DSC) was performed on a TA instrument DSC 2920, at a scan rate of 10 °C min^{-1}.

Small-angle neutron scattering experiments have been performed on the PACE spectrometer (LLB, Saclay). Three configurations (wavelength $\lambda_0 = 6.0$ Å, $D_{\text{sample-to-detector}} = 1.24$ and 4.57 m, and $\lambda_0 = 16.8$ Å, $D_{\text{sample-to-detector}} = 4.57$ m) were used, covering a q-range of 0.003−0.26 $Å^{-1}$. Data treatment was done with a homemade program (Pasidur, LLB) following standard procedures,[9] with H_2O as calibration standard. Incoherent background was determined with several H/D mixtures and interpolated for the desired concentrations. The absolute values of the scattered intensity (in cm^{-1}) were measured via a determination of the direct beam intensity.

Silanization of Colloidal Silica Nanoparticles in Dimethylacetamide. The silica dispersion (52.7 g of 20 wt % SiO_2 in dimethylacetamide) was added to a 250 mL round-bottom flask with a magnetic stir bar and fitted with a reflux condenser. Mercaptopropyl triethoxysilane (MPTS) (0.7 mL, 3.15 mmol) was added, and the reaction mixture was gently refluxed for a period of 4 h. Maximum grafting was obtained after that time, and the percentage of silane condensed on the surface of silica nanoparticles was determined from elemental analysis of sulfur.

Overgrafting of 2-Bromoisobutyrate Bromide onto the Thiol-Functional Silica Nanoparticles. DMAP (0.17 g, 1.4 mmol) and DMAc (40 mL) were introduced in a three-neck flask under nitrogen. Next, 10 mL of the previously silanized particles dispersion in DMAc was added through a filter (0.45 μm) to obtain a 4 wt % SiO_2 solution. 2-Bromoisobutyrate bromide (0.32 g, 1.4 mmol) diluted in 10 mL of DMAc was then added dropwise to the reaction mixture. The amount of DMAc added to the final solution mixture was adjusted to dilute the solution to 3.5 wt % of SiO_2. The solution was stirred and heated. Different temperatures were used as well as other bases than DMAP (see Table 1). After 48 h, the reaction mixture was filtered under gas pressure using a Millipore Ultrafiltration apparatus with a 30 000 Da pores diameter filter (regenerated cellulose) provided from Millipore. The solution was filtered four times. Each time, 50 mL of the obtained solution was diluted with 300 mL of DMAc and then reconcentrated to the initial volume.

Determination of the Number of Initiation Sites. The number of initiator molecules grafted onto the surface of the nanoparticles is correlated to the number of bromine atoms obtained from elemental analysis according to the following equation:

$$\text{no. of molecules per nm}^2 = \frac{n_{\text{Br}} \times N_{\text{A}}}{A \times 10^{18}} \qquad (1)$$

where N_A is Avogadro's number, A is the specific area of the silica particles in nm^2, and n_{Br} is the number of moles of bromine determined from elemental analysis relative to the amount of silicone atoms.

Model Polymerization in Solution. Synthesis of (2-Bromo-thioisobutyrate)propane. Soluble initiator was prepared by mixing in a 100 mL three-neck flask, 4.75 mL of propanethiol (52.5 mmol) and 5.09 mL (63 mmol) of pyridine in 50 mL of dry THF. Next, 7.8 mL (63 mmol) of 2-bromoisobutyrate bromide was added dropwise at 0 °C. The reaction proceeded under nitrogen at 0 °C for 1 h followed by 48 h at room temperature. The crude product was then isolated by filtration, and the solution mixture was extracted from a 2 N hydrogen chloride solution, after dilution in hexanes. The solution was washed twice with water, dried over sodium sulfate, and the solvent evaporated. The product could be further distilled and was analyzed by ^{1}H NMR ($CDCl_3$): δ 0.995 (t, 3H, CH_3); δ 1.63 (m, 2H, CH_2); δ 1.95 (s, 6H, $(CH_3)_2$); δ 2.88 (q, 2H, CH_2).

Using (2-bromo-thioisobutyrate) propane previously synthesized as an initiator and the CuBr/pentamethyldiethylenetriamine (PMDETA) as the catalyst system, ATRP of styrene was performed in 25% DMAc solution by volume. A typical polymerization procedure is as follows. All liquids were deoxygenated by bubbling with nitrogen for 30 min. To a three-neck round-bottom flask (previously purged by several vacuum/N_2 cycles) were added (final concentrations are given in parentheses) 67 mg (0.027 M) of Cu^IBr (stored under nitrogen), 4.6 mL of DMAc, and 0.1 mL (0.027 M) of PMDETA. The mixture was stirred at room temperature until all copper bromide had been solubilized. Once the reaction mixture was homogeneous, 17 mL (8.6 M) of styrene and 0.14 mL (0.046 M) of initiator were added. The CuBr/PMDETA/initiator molar ratio was 0.6:0.6:1. An initial sample was taken via a nitrogen-purged syringe, and then the reaction flask was heated to 110 °C and remained under continuous nitrogen purge. Kinetic samples were taken via purged syringes and were used to determine conversion by gravimetry. Molar mass evolution was obtained from gel permeation chromatography (GPC), after the samples had been purified through an alumina column to remove the copper derivative.

ATRP of Styrene from 2-Bromo-thioisobutyrate Nanosilica Colloids (BIB-SiO_2). Colloidal initiators of silica ($BIBSiO_2$) in DMAc (20 mL of a 3.5 wt % SiO_2 sol), Cu(I)Br (26 mg, 0.18 mmol), and PMDETA (31.5 mg, 0.18 mmol) were

Scheme 1. Grafting of the Initiator Molecule via the "Overgrafting Method"

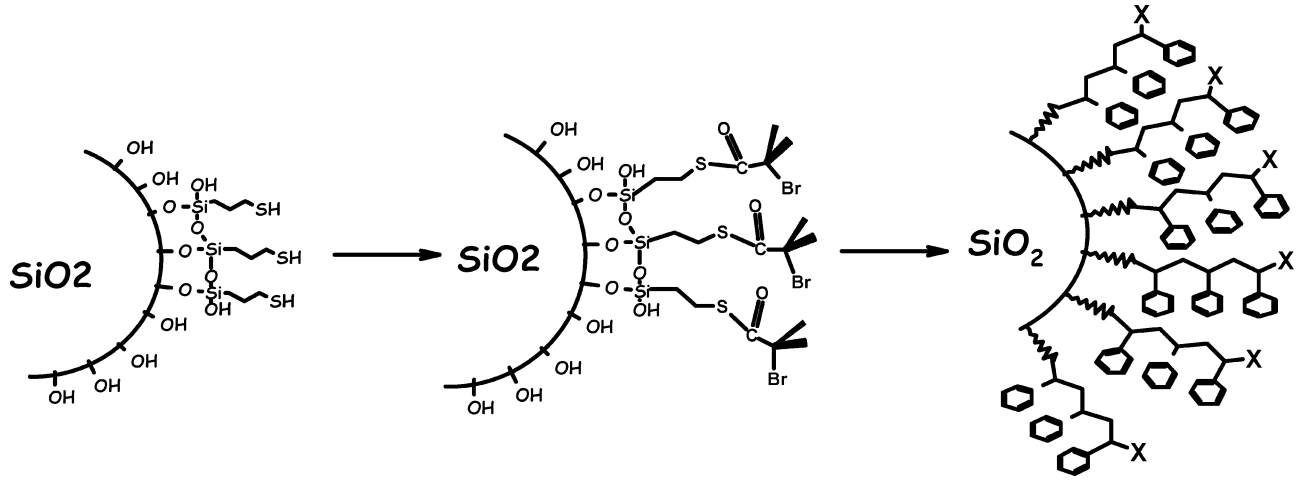

added to a 250 mL three-neck flask under nitrogen. The CuBr/PMDETA/BIBSiO$_2$ molar ratio was 0.6:0.6:1. Some free initiator (the same molecule as the one used in the solution polymerization) was also added to the solution (34 mg, 0.15 mmol). All liquids were deoxygenated by bubbling with nitrogen for 30 min. The reaction mixture was stirred until it became homogeneous. Styrene (35 mL, 0.3 mol) was added dropwise within the first hour, to avoid gelification which could be induced by the change in polarity of the solvent mixture. The reaction flask was then heated to 110 °C. Kinetic samples were taken via purged syringes and were used to determine conversion by gravimetry. Molar mass evolution was obtained from gel permeation chromatography (GPC), after sample purification through precipitation in methanol.

As soluble initiator was added to the reaction mixture, free polymer was extracted using centrifugation at 16 000*g*. The supernatant was removed, and the presence of polymers was checked by infrared spectroscopy. The solution was recentrifuged until no more polymer was detected.

Results and Discussion

Grafting of the Initiator. This reaction was performed in two steps (Scheme 1). Both were conducted in dimethylacetamide (DMAc), the solvent in which the particles are dispersed. The first step involved the silanization of the particles with a thiol-containing silane. The second one was an "overgrafting" reaction which consisted of an esterification of the thiol group with the 2-bromoisobutyrate bromide. This procedure permits one to adjust with a certain accuracy the degree of grafting that may be varied from 0.5 to 5 molecules/nm^2.

The first step was a straightforward reaction, easy to control. The use of a triethoxysilane was favored because the grafting is more efficient as compared to a monoethoxysilane. Now, the drawback is the possibility to generate a polycondensed silane network. Thus, the structure of the mercaptopropyl triethoxysilane (MPTS) layer onto the silica nanoparticles, depending on the degree of grafting, was investigated from ^{29}Si CP/MAS NMR (Figure 1). We introduced in the batch either 6 or 30 wt % of MPTS (with respect to dried silica particles) corresponding to either 1 or 5 molecules/nm^2, respectively. Theoretically, a concentration of 30 wt % of silane corresponds to one MPTS for one hydroxy group of the silica surface, whereas a concentration of 6 wt % of silane leads to one MPTS for 5 OH groups. From ^{29}Si CP/MAS NMR, it is possible to differentiate the different types of silicon atoms present in the silica particles: Q^4, Q^3, and Q^2, that is, in the bulk, on the surface bonded

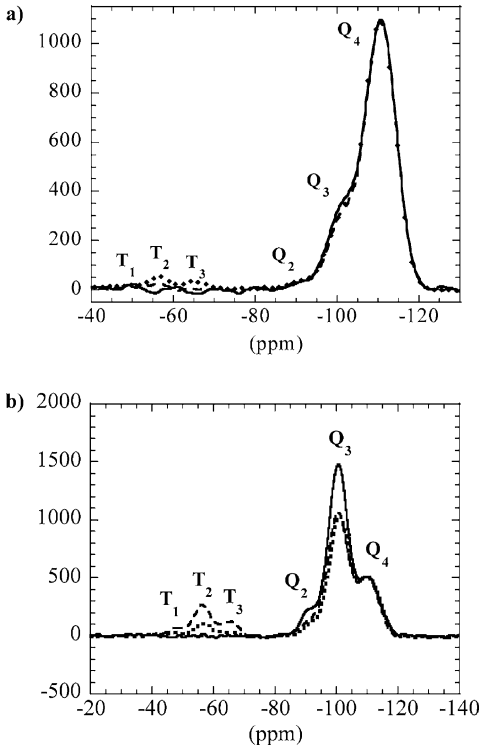

Figure 1. Solid-state ^{29}Si CP/MAS NMR spectra of the naked silica nanoparticles (−), the thiol-functionalized silica nanoparticles with 1 silane/nm^2 (- - -), and the thiol-functionalized silica nanoparticles with 5 silanes/nm^2 (− −). (a) Simple impulsion. (b) Cross-linked polarization.

to one OH and to two OH, respectively. The patterns T^1, T^2, and T^3 correspond to the silicon atoms contained in the silane molecule which have formed one (or two, or three, respectively) Si−O−Si bond with the silica particle, or one Si−O−Si binding between two silanes. In Figure 1a and b (spectra of Figure 1b have been magnified for the sake of clarity), we show the spectra of the original silica particles, of the silica particles treated with 6 wt % of MPTS, and of the silica particles treated with 30 wt % of MPTS. In the figure, the chemical shifts of the Q^4, Q^3, and Q^2 silicon nuclei were observed as a trimodal signal at −111, −101.5, −92 ppm. When the MPTS is added, signals due to the T^2 and T^3 patterns appear at −56 and −65 ppm, respectively. The comparison of the increase in intensity for the (T^2 + T^3) peaks with the decrease of the Q^3 one (as

Scheme 2. Structure of the Condensed Silane on the Surface of the Silica Nanoparticle: (a) Grafted Silane Monolayer Obtained from the Condensation of 1 Silane per nm^2; (b) Polycondensed Silane Layer Obtained from the Condensation of 5 Silane per nm^2

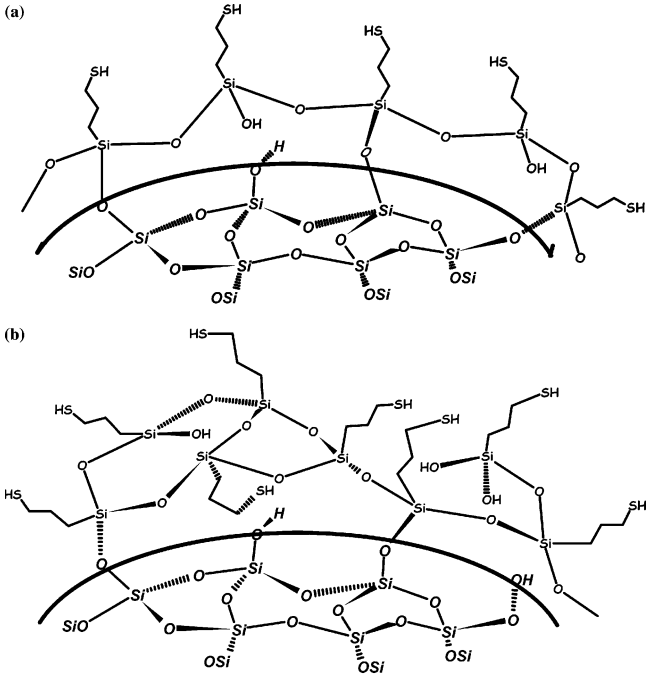

compared to the original silica particle spectrum) allowed one to deduce the amount of polycondensed silane. In the case where 6 wt % of MPTS is added to the silica sol, integration over the T^2 and T^3 peaks displays an increase (with respect to untreated silica) which is twice the decrease in integrated intensity over the Q^3 peak. This means that we have one Si−O−Si bond to the surface for two polycondensed silanes. This is equivalent to the formation of a monolayer. In the case where 30 wt % of MPTS is added to the silica sol, the intensity of ($T^2 + T^3$) peaks increases, but the Q^3 one is the same as that for the 6 wt % MPTS addition. Thus, when adding 30% MPTS, we get one Si−O−Si surface binding for 8 polycondensed silicons.

Quantitative measurements of the grafting efficiency can be obtained from the elemental analysis of sulfur. They were found to be close to 100% in the case of a reaction with the equivalent of 1 silane/nm^2 (Table 1). In conclusion, we have ensured that grafting one silane per nm^2 or less (characterization of the layer with 0.5 silane per nm^2 has been done) led to the formation of a monolayer.

The second step, which consists of an overgrafting of the initiator moiety onto the prefunctional particles,

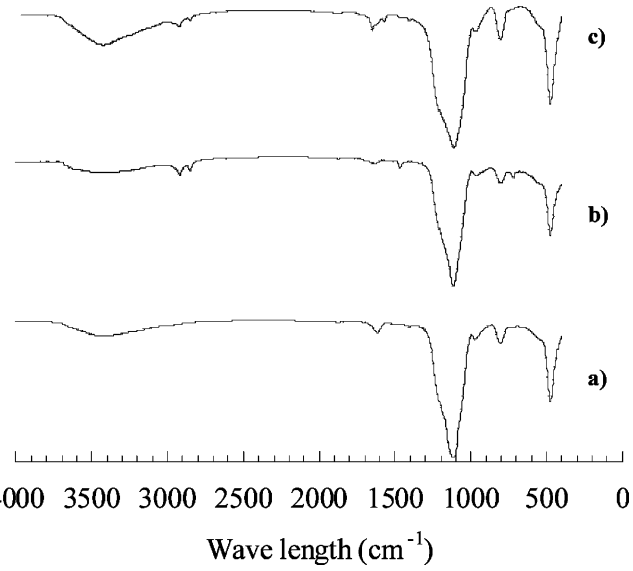

Figure 2. FT-IR spectra of the naked silica nanoparticles (a), and the particles grafted from mercaptosilane (b), and from (2-bromo-thioisobutyryl) propane (c).

turned out to be more difficult. Running the esterification reaction in a colloidal suspension of silica nanoparticles in DMAc cannot be done as usual. In particular, the addition of the basic catalyst was the critical point: most of the common bases, like triethylamine or pyridine, were found to be inefficient or to cause the formation of a gel due to aggregation of the nanoparticles.

Table 1 reports the different percentages of initiator grafted onto silica particles (these values are calculated from elemental analysis). The use of a more powerful base, (dimethylamino)pyridine (DMAP), gave the most satisfactory results, especially when the reaction was conducted at 80 °C (grafting of the initiator moiety was 100% as compared to the initial amount of thiol functions). It is reported in the literature that the better catalytic effect is not only due to the higher pK_a, but also to the higher stability of the formed salts.[10a] Other attempts have been conducted using another catalytic system based on (dimethylamino)pyridine-toluenic sulfonate (DPTS) synthesized according to a procedure described elsewhere.[10b] We expected the reaction to be efficient at room temperature, but actually the results were not as good as those with the DMAP at 80 °C. The reaction was conducted for 6 h and purified from ultrafiltration to avoid any drying of the particles and to keep the particle in solution.

Infrared spectroscopy was carried out to account for the successful grafting (Figure 2). After addition of the

Table 1. Overgrafting of (2-Bromoisobutyryl)bromide: Characterization of the Functionalized Particles after Reactions with Different Bases

entry	base reactant, molar equiv[b]	T °C[b]	no. of intiator/nm^2 theo.	no. of sulfur/nm^2 [a]	no. of bromide/nm^2 [b]	mmol of initiator/g of sample	observations
1A	pyridine, 4.8	25	4	2.9	0.18	4.1×10^{-2}	yellow coloration
2A	Et_3N, 3.6	25	1	0.98	0.5	1.7×10^{-1}	gel formation
2B	pyridine, 3.6	80	1	0.98	0.52	1.8×10^{-1}	gel formation
3A	DPTS, 5[c]	25	5	3	0.6	1.36×10^{-1}	
3B	DPTS, 1[c]	25	5	3	0.44	10^{-1}	
4A	DMAP, 3.6	25	1	0.87	0.15	3.5×10^{-2}	
5B	DMAP, 3.6	50	1	0.95	0.53	1.19×10^{-1}	
2C	DMAP, 3.6	80	1	0.98	1.02	2.32×10^{-1}	

[a] After the silanization reaction. [b] During and after the overgrafting reaction (molar equiv are calculated with respect to the amount of SH/nm^2). [c] In that case, the esterification reaction is done using 2-bromo-2-methylpropionic acid and dicyclohexylcarbodiimide (DCC).

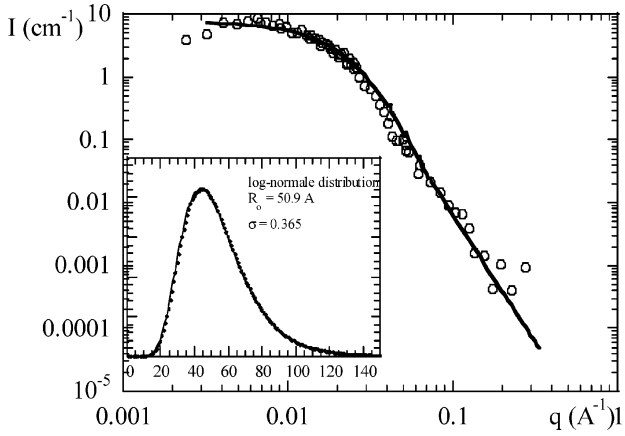

Figure 3. Small-angle neutron scattering from the initial silica dispersion in DMAc ($\Phi_{si} = 0.25\%$).

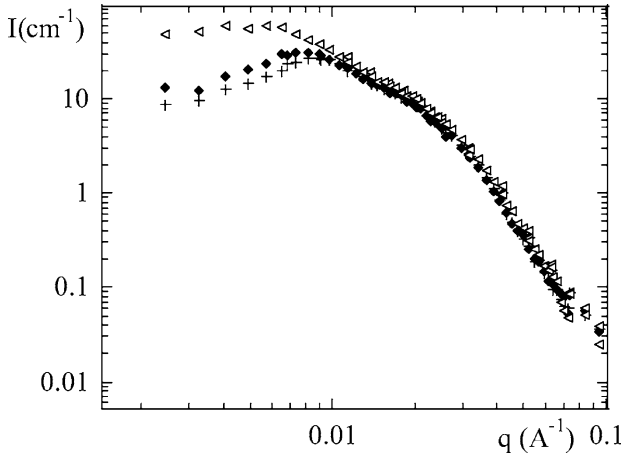

Figure 4. Small-angle neutron scattering from the silica dispersion at the different stages of the functionalization of the particles ($\Phi_{si} = 1\%$): (+) naked silica particles, (◆) thiol-functional silica particles, and (<) initiator-overgrafted silica particles.

mercapto-silane (spectrum b), we observed only absorption bands due to the C−H stretching (2850−2950 cm^{-1}). The presence of the thiol group could not be characterized from IR, as it absorbs preferentially in Raman. Nevertheless, spectrum c (overgrafting reaction) showed the presence of the carbonyl absorption band (1690 cm^{-1}) attesting the presence of the thioester group.

Colloidal Stability after Grafting of Initiator. Small-angle neutron scattering (SANS) was used to check the preservation of the colloidal stability through the different reaction steps. This technique is particularly appropriate for the characterization of such systems for several reasons: range of scales attainable, index matching between the solvent and the particle, or the polymer chains. For the first time, we have characterized the untreated nanosilica beads by measuring the scattered intensity in dilute solution ($\Phi_{si} = 0.25\%$) in DMAc. In Figure 3, this experimental result is compared to a model calculation of the form factor of polydisperse spherical silica beads. A log-normal size distribution was chosen, and the parameters of the fit are $R_o = 50.9$ Å and $\sigma = 0.365$. The resolution function of the spectrometer is also taken into account. The rather broad polydispersity (high σ) of the spheres is in line with the absence of any oscillation in the intermediate q-range. The corresponding radius distribution function is plotted in the inset. Note that the log-normal size distribution was chosen for convenience only. We do not claim that the size of our silica beads really follows this distribution, but just that their scattering is compatible with it. It is clear from the data, however, that the typical sizes are in the 100 Å range, whatever the distribution chosen to describe the data.

We now turn to the discussion of the spectra measured at different steps of the grafting procedure. In general, SANS spectra of hairy particles are rather complicated,[11] as they involve the interparticle structure factor, the scattering from the silica core and the hairy layer, as well as the cross-correlation terms. In the present work, we were not interested in such a detailed description, but made use of the maximum of the intensity. Indeed, in the presence of repulsive interactions between particles, for example, of electrostatic or steric origin, a peak in the intensity is generally observed. It is due to the maximum of the interparticle structure factor, which is the Fourier transform of the particle−particle correlation function. The peak position q_o is directly related to the most probable distance between particles $D = 2\pi/q_o$ and can be used to estimate the volume of the particles V_{si}:

$$V_{si} = \Phi_{si} D^3 \qquad (2)$$

Here Φ_{si} denotes the volume fraction of particles. Therefore, the peak position can be used directly as an estimation of the level of particles aggregation in the sample at the different steps of the grafting. Note that this method relies on the hypothesis that the interaggregate structure in solution is approximately cubic. In a liquid, this is generally not true, and a systematic error in the estimation of V by means of eq 2 is therefore introduced. Another indication of aggregation is a higher intensity at low-q. In the absence of interactions between aggregates, $I(q \rightarrow 0)$ is proportional to the volume of aggregates.

Applying eq 2 to the scattering of the dilute silica solution, we estimated a bead volume of 2.2×10^6 $Å^3$. For a monodisperse sphere, this corresponds to a radius of 81 Å, consistent with the radius size distribution function shown in Figure 3. The SANS intensities of pure silica beads, after silanization, and after overgrafting, were compared in Figure 4. The scattering of untreated silica dispersion at $\Phi_{si} = 1.0\%$ is typical of a colloidal dispersion. Starting from low-q, the intensity first rose to a peak located at $q = 0.009$ $Å^{-1}$, which is the signature of repulsive interactions, presumably of electrostatic origin. This peak position compared favorably to the value of 0.01 $Å^{-1}$ which could be predicted from the particle volume measured from the dilute solution. At high-q, the intensity decreased with a q^{-4} power Porod law typical for a well-defined interface between silica and solvent. Upon silanization, the structure was hardly modified in the q-range of observation. Note that this range corresponds to sizes ranging from a few angströms up to several hundred angströms; that is, aggregation of silica beads can be detected with these experiments. Minor changes in the low-q intensity speak in favor of a minor modification of the interparticle interactions, up to maybe some very limited aggregation (average aggregation number less than 2). At high scattering vectors, intensities superimposed rather well, which was expected given the small quantity of thiol-functional groups present at the interface (with respect to the mass of the silica beads) and given the

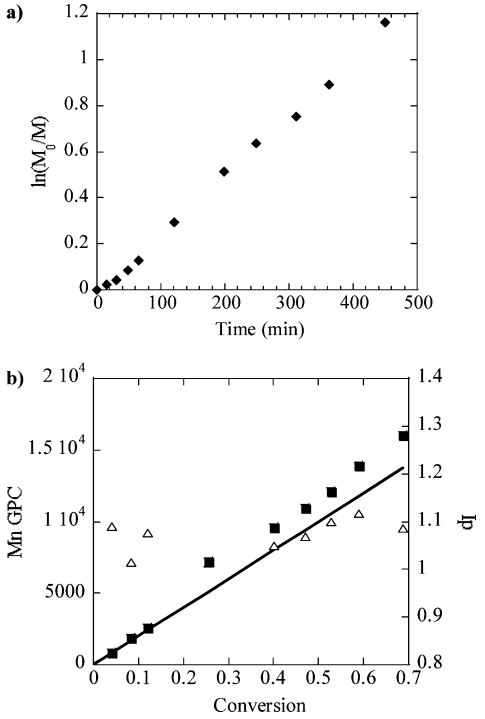

Figure 5. Solution−atom transfer radical polymerization of styrene in dimethylacetamide (DMAc) using (2-bromothioisobutyrate) propane at stoichiometric ratios of 189:1:0.6:0.6 for [styrene]:[I]:[Cu(I)]:[PMDETA] at 110 °C; (a) semilogarithmic plot of monomer conversion versus time (◆), (b) plots of M_n and M_w/M_n (Ip) versus conversion (■;△).

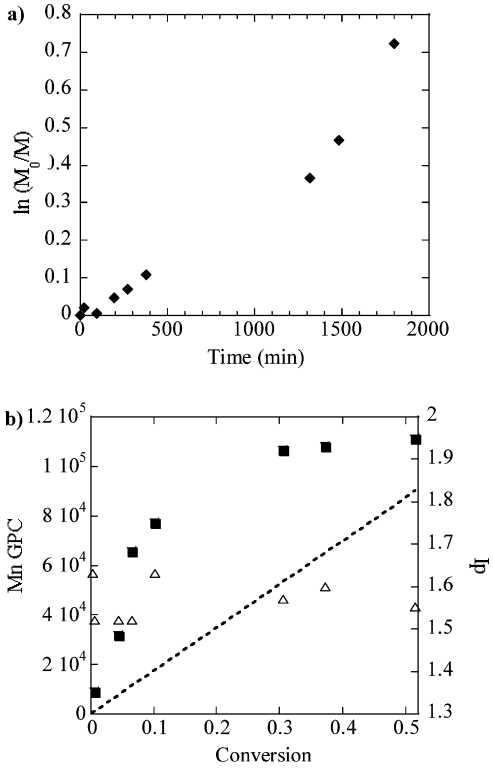

Figure 6. Atom transfer radical polymerization of styrene from silica nanoparticles: analysis of the free chains at stoichiometric ratios of 1670:1:1:1 for [styrene]:[I]:[Cu(I)]:[PMDETA]; (a) semilogarithmic plot of monomer conversion versus time (◆), (b) plots of M_n and M_w/M_n (Ip) versus conversion (■;△).

poor contrast of such moieties with respect to the solvent (which was not deuterated).

Once the initiator was grafted (overgrafting), the intensity was somehow higher in the low-q range, while there were still virtually no changes at high-q. The maximum intensity about doubled (from 32 to 60 cm^{-1}), and the interaction peak broadened and shifted to lower q-values. This behavior was compatible with a slight aggregation of two or three beads per aggregate (on average). We conclude that the solutions staid in the state of a well-controlled colloidal dispersion during these first two steps of the grafting.

Polymerization. Before conducting the polymerization from the silica nanoparticles surface, we needed to ensure that polymerization could be done in the conditions imposed by the colloidal solution (solvent, concentration, etc...). Thus, we conducted a polymerization in solution without silica particles. Solution polymerization of styrene in DMAc (25 wt %) using (2-bromo-thioisobutyrate) propane as the initiator allowed us to account for the influence of the solvent and the initiator structure (presence of the sulfur) on the polymerization and to determine the most appropriate molar ratio of copper, ligand, and initiator. We show, in Figure 5, the results obtained for a ratio of [Cu(I)Br]:[PMDETA]:[I] of 0.6:0.6:1. The semilogarithmic plot of monomer consumption with time is linear as well as the plot of number-averaged molecular weight (M_n) versus conversion where the M_n values were very close to the theoretical ones. This proves that polymerization of styrene in these conditions has the characteristics of a controlled/"living" polymerization. Moreover, the molecular weight distribution remained very narrow throughout the polymerization process.

After that, the polymerization from 2-bromo-thioisobutyrate silica particles (BIB-SiO_2) was performed. In addition to the grafted initiator, some free molecular initiator was added in the dispersion. As shown before,[7c,8a] this should ensure the necessary amount of Cu(II) for the control of the molecular mass. The concentration imposed by the colloidal suspension would lead to a very low concentration of initiator, if only grafted initiator was present. Moreover, the presence of the free chains did facilitate the GPC analysis of the molecular mass. Under such conditions, the polymerization kinetics of styrene from silica colloidal initiator has been investigated (Figure 6).

Polymerizations were carried out in dimethylacetamide (3 wt % of silica) with a high molar ratio of monomer to initiator molecules (grafted or nongrafted) to keep a percentage of solvent relative to monomer close to 25 wt %. The polymerization could be maintained to high conversion (reaction time ≥ 24 h) without interparticle coupling leading to gelation. Let us stress that particles are far from each other due to very low particle concentration. This prevents coupling between chains grafted on two different particles. The semilogarithmic plot of monomer conversion with time is linear during the whole polymerization process, attesting that a certain control has remained. The plot of number-averaged molecular weight versus conversion is also linear, but the experimental molecular weights were higher than the theoretical ones, especially at low conversion. This reveals a low initiation efficiency. Figure 7 shows the plot of the initiation efficiency versus the conversion where a quasi-linear increase of the efficiency is observed. At the beginning of the polymerization (conversion ≤ 10%), the initiation efficiency was very low (less than 25%). It then increased while the polymerization proceeded to reach more than 80% at

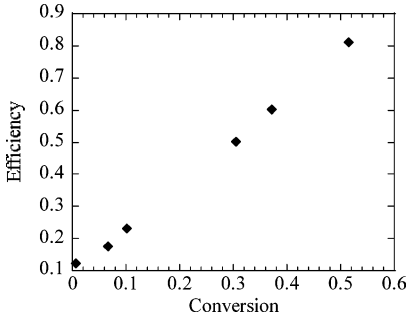

Figure 7. Initiation efficiency calculated from the ratio of $M_{n,theoretical}$ ($[M]_0/[I]_0 \times$ conversion $\times$ $FW_{monomer}$) and $M_{n,SEC}$ versus monomer conversion.

the end of the polymerization. This can be explained by the formation of new chains during the polymerization. Similar behavior has been observed for the polymerization from silica particles, and it has been explained by steric congestion of initiator groups.[8a,g] In the present case, this effect could also be due to the high dilution of the species. Indeed, this low concentration of initiation sites and the difficult access to the grafted initiator could explain the variation in the initiation efficiency. Nevertheless, the polydispersity index did not increase with the conversion and remained quite stable through the polymerization ($1.5 \leq M_w/M_n \leq 1.6$).

Table 2 reports the results obtained from polymerization of styrene from silica colloidal initiator. Grafted polymer chains have been analyzed from GPC after etching with HF, following the procedure given by Patten.[8a] It was found that molecular weights of the grafted chains were slightly higher than those of the free chains. Steric congestion of initiators onto the surface of particles may represent an important contribution in the reduction of the initiation efficiency. Not all initiator sites at the nanoparticles surface were efficient. The growing chains may sterically hinder the access of the catalyst to the neighboring initiation sites on the particle surface. Nevertheless, the polydispersity (M_w/M_n) was also lower for the grafted chains, as compared to that of the free chains. This can be explained by the fact that the polymerization is conducted at a temperature where thermal polymerization of styrene can occur. That involves the presence of noncontrolled chains in the solution that would increase the polydispersity index of the "free" chains. Patten[8a] has also mentioned that termination reactions occur predominantly in solution (presence of two diffusing chains).

The two chromatograms shown in Figure 8 were obtained from a GPC instrument coupled to a refractive index and a dynamic light scattering detector (static light scattering signals are not shown for clarity). The grafted particles with the free polymers have been injected directly (after copper removing, drying, and dilution in THF). Chromatograms a and b in Figure 8 represent two samples taken at different monomer conversions ($a = 6\%$; $b = 51\%$). Chromatogram a showed the presence of the free chains (with signals both from the refractive index and from the light scattering detector) and a second peak (at lower elution time) arising only from the dynamic light scattering detector which could only be due to the presence of the grafted silica particles. The quantity of polymer attached to these particles was lower than the refractive index detection threshold. In chromatogram b, one could observe a signal appearing from the refractive index in the same area of this second peak. This means that some polymers attached to the objects were responsible for this signal. The indicated R_h value of the order of 40 nm was similar to that obtained from classical light scattering measurements done on our polymer-grafted particles after they were washed from free chains using centrifugation (Table 2). This shows that some polymers were attached to the particles and that the particles could be redispersed, even after being dried. The attached polystyrene helps for the redispersion.

The amount of polystyrene grafted onto the particles has been estimated from thermogravimetric analysis and was found to be 49.36% (sample 1 in Table 2). In this case, this corresponded to a total of 55 chains per nanoparticles.

The structure of the samples during the polymerization from the particles has been investigated by SANS. In Figure 9, the intensity scattered by a sample in nondeuterated DMAc ($\Phi_{si} = 0.83\%$) after 4 h of polymerization is compared to the one of pure silica beads in the same solvent. The volume fraction of scattering objects being a prefactor of the form factor measured at such high dilutions, we have plotted I/Φ_{si} for direct comparison. The intensities were shown to superimpose at high-q, while a significant deviation was observed at low-q. After 4 h of polymerization, aggregation of the silica was observed, as could be inferred from the absence of a low-q plateau, replaced by a continuous increase with a power law close to q^{-2} in this range. From the highest intensity and the lowest q-value, we could deduce that the aggregation number is at least several tens. This aggregation observed in the case of polymerization of styrene could be attributed to the low polarity of this monomer, which lowered the polarity of the suspension in DMAc. A different behavior has been observed with another monomer, and results will be shown in a forthcoming paper.

In a second, more explorative experiment, we have tried to follow the kinetics of polymerization from the silica particles, in a time-resolved SANS experiment. At different stages of the polymerization, samples were taken out and immediately cooled to stop the reaction. For all samples, we used a mixture of nondeuterated and deuterated DMAc which has the same scattering length density (i.e., the same index) as silica. Therefore, the silica signal should be null, allowing the detection of the polymer. In Figure 10, the results obtained from the polymerization immediately after addition of monomer, after 15 min , and 1, 2, and 3 h of reaction, are plotted. Note that after 30 min, no more monomer is added to the solution; for the corresponding last three curves, the silica concentration is constant.

The signal is very low, especially in the high-q range where background subtraction of these samples of different chemical composition decreases the accuracy of the data. Nonetheless, all samples show a signal typical for the silica bead at intermediate q-values. Due to the use of a mixture of nondeuterated and deuterated DMAc, the signal from pure silica should be null. However, the presence of styrene monomer (nondeuterated) added to DMAc modifies the solvent index. Therefore, the contrast of silica becomes larger than zero (but still 10 times less than for silica in h-DMAc). However, when polymerization proceeds, the monomer is transformed into polymer, a part of which we expect

Table 2. GPC Data for the Atom Transfer Radical Polymerization from Silica Nanoparticles in Dimethylacetamide

entry	conditions[a]	no. initiator/nm^2	moles equiv of initiator in sol.	reaction time (h)	conv (%)[b]	$M_{n,SEC}$[c]	M_w/M_n	Rh (DLS) nm	$M_{n,SEC}$ of cleaved chains[d]
1	1670:1:1:1	0.15	6.67	30	50	106 600	1.55	41	132 000 (1.28)
2	1340:0.8:0.8:1	0.56	1.79	21	43.5	127 000	1.51	44	144 100 (1.32)
3	775:0.6:0.6:1	0.5	6	4	5.1	32 000	1.76	39	
4	1460:0.6:0.6:1	0.5	3	4	8	48 600	1.61	58	66 000 (1.48)

[a] Conditions correspond to molar ratios of monomer, 2-bromothioisobutyrate group on the silica colloid and in solution, Cu(I)Br, and PMDETA (ratios have been calculated from values given by elemental analysis). [b] Conversion values are determined from gravimetric analysis. [c] Molecular weight of polymer chains formed in solution. [d] Molecular weight and molecular weight distribution in brackets, of grafted polymer chains after etching with HF.

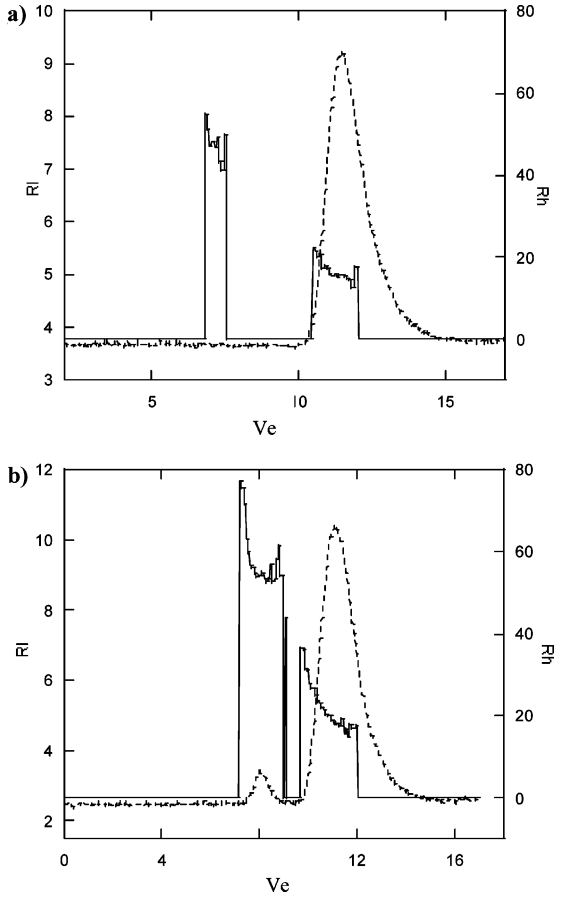

Figure 8. SEC chromatograms obtained from (- - -) the refractive index detector, and (−) the dynamic light scattering detector for 6% (a) and 51% (b) conversion.

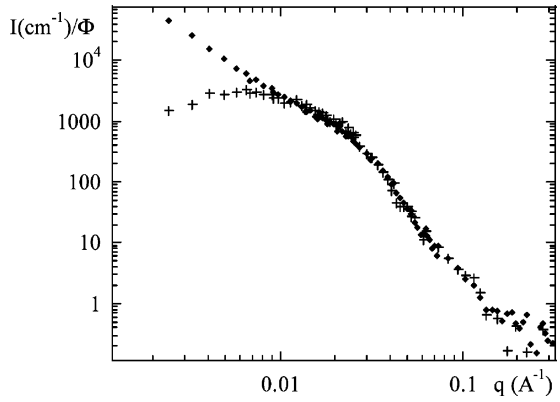

Figure 9. Small-angle neutrons scattering intensity after 4 h of polymerization (+) as compared to the naked silica particles (◆) (Φ_{si} = 0.8%).

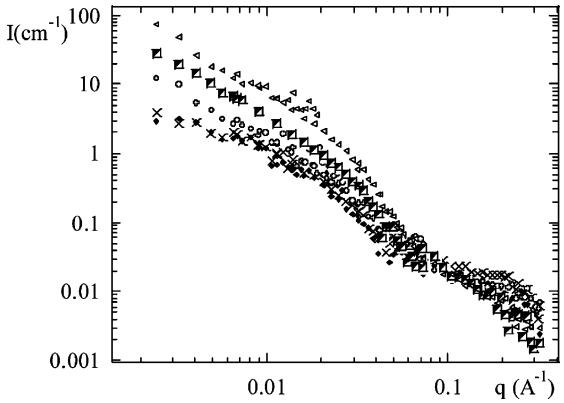

Figure 10. Kinetics study of the polymerization from the silica nanoparticles by small-angle neutron scattering. After reaction times of: (◆) 0 min; (×) 15 min; (<) 60 min; (□) 120 min; and (◇) 180 min.

to be located around the silica. Therefore, the silica contrast should decrease. This can explain the decrease of the signal observed at the largest q. On the contrary, at small and intermediate q's, we observe that the signal is increasing! At the lowest q's, this is certainly signaling aggregation, because the curve shape becomes different (the onset of plateau is transformed into a slope, similarly to the q^{-2} power law observed for Figure 9). At intermediate q, conversely, the increase of the signal is probably not due to aggregation, because the curves keep their curvature around 0.02−0.03 Å^{-1}, which is characteristic for the silica beads. This feature is an important clue for attributing this signal to some polymer attached to the silica surface: the nonzero contrast of the polymer increases the effective signal from the particles. Recent measurements on polymerization from another monomer show the same behavior.

Conclusions

We have described a new route for preparing ATRP initiator-grafted nanoparticles. By this work, we showed that every step of surface modifications and polymerization could be done while keeping the silica nanoparticles in solution. This is the only way to keep them well-dispersed and to avoid aggregation. Ultra-filtration was used as the method for purification, and the dispersion of the particles was checked from light and neutron scattering at every stage of the functionalization, attesting for the nonaggregation of the particles. Atom transfer radical polymerization of styrene has been successfully conducted from these particles, showing a good control despite the dilution conditions (necessary to keep the particles apart from each other) and the complex nature of the initiation from the particles. A

SANS kinetic study of the polymerization has showed that aggregation of polymer-grafted particles was progressively and gently increased, while the signal at intermediate length scale could be explained by the increase in thickness of the polymer layer. The next step is to see whether these hybrids nanoparticles give rise to new mechanical properties once incorporated in a polymer matrix. This is currently under study.

Acknowledgment. We thank France Costa-Torro (LCM, CNRS/Université Pierre et Marie Curie) for the thermogravimetric analysis. We are also grateful to Ivan Klur and Armelle Pourpoint for solid-state ^{29}Si CP/MAS NMR (Rhodia, Centre de Recherche d'Aubervilliers) analysis. Support of this work by Région Ile de France, CEA, and Rhodia is greatly acknowledged.

References and Notes

(1) (a) Mark, J. E.; Erman, B. *Science and Technology of Rubber*; Academic Press: San Diego, 1994. (b) Nielsen, L. E.; Landel, R. F. *Mechanical Properties of Polymers and Composites*; Marcel Dekker: New York, 1994. (c) Edwards, D. C. *J. Mater. Sci.* **1990**, *25*, 4175. (d) Voet, A. *J. Polym. Sci.: Macromol. Rev.* **1980**, *15*, 327.

(2) Iler, R. K. *The Chemistry of Silica: Solubility, Polymerization, Colloïd and Surface Properties, and Biochemistry*; Wiley-Interscience Publ.: New York, 1979.

(3) (a) Oberdisse, J.; Demé, B. *Macromolecules* **2002**, *35*, 4397−4405. (b) Oberdisse, J. *Macromolecules* **2002**, *35*, 9441−9450.

(4) Overbeek, J. T. G. *Colloidal Dispersions*; Royal Society of Chemistry: London, 1981.

(5) (a) Prucker, O.; Ruhe, J. *Macromolecules* **1998**, *31*, 602−613. (b) Prucker, O.; Ruhe, J. *Macromolecules* **1998**, *31*, 592−601.

(6) (a) Patten, T. E.; Matyjaszewski, K. *Adv. Mater.* **1998**, *10*, 901. (b) Xia, J.; Zhang, X.; Matyjaszewski, K. *Macromolecules* **1999**, *32*, 3531.

(7) (a) Ejaz, M.; Shinpei, Y.; Kohji, O.; Tsujii, Y.; Fukuda, T. *Macromolecules* **1998**, *31*, 5934. (b) Huang, X.; Wirth, M. J. *Macromolecules* **1972**, *5*, 1694−1696. (c) Husseman, M.; Mamstrom, E.; McNamara, M.; Mate, M.; Mecerreyes, D.; Benoit, D.; Hedrick, J.; Mansky, P.; Huang, E.; Russell, T.; Hawker, C. *Macromolecules* **1999**, *32*, 1424. (d) Matyjaszewski, K.; Miller, P. J.; Shukla, N.; Immaraporn, B.; Gelman, A.; Luokala, B.; Siclovan, T.; Kickelbick, G.; Vallant, T.; Hoffmann, H.; Pakula, T. *Macromolecules* **1999**, *32*, 8716. (e) Zhao, B.; Brittain, W. J. *J. Am. Chem. Soc.* **1999**, *121*, 3557. (f) Shah, R. R.; Merreceyes, D.; Husemann, M.; Rees, I.; Abbott, N.; Hawker, C.; Hedrick, J. L. *Macromolecules* **2000**, *33*, 597−605. (g) Ejaz, M.; Ohno, K.; Tsujii, Y.; Fukuda, T. *Macromolecules* **2000**, *33*, 2870−2874. (h) Kong, X.; Kawai, T.; Abe, J.; Iyoda, T. *Macromolecules* **2001**, *34*, 1837−1844. (i) Mori, H.; Böker, A.; Krausch, G.; Müller, A. H. E. *Macromolecules* **2001**, *34*, 6871. (j) Xiao, D.; Wirth, M. J. *Macromolecules* **2002**, *35*, 2919−2925. (k) Carlmark, A.; Malmström, E. *J. Am. Chem. Soc.* **2002**, *124*, 900−901. (l) Kim, J.-B.; Huang, W.; Bruening, M. L.; Baker, G. L. *Macromolecules* **2002**, *35*, 5410−5416.

(8) (a) Von Werne, T.; Patten, T. E. *J. Am. Chem. Soc.* **2001**, *123*, 7497−7505. (b) Zheng, G.; Stöver, H. D. H. *Macromolecules* **2002**, *35*, 6828−6834. (c) Vestal, C. R.; Zhang, J. *J. Am. Chem. Soc.* **2002**, *124*, 14312. (d) Mori, H.; Chan Seng, D.; Zhang, M.; Müller, A. H. E. *Langmuir* **2002**, *18*, 3682. (e) Gu, B.; Sen, A. *Macromolecules* **2002**, *35*, 8913. (f) Ohno, K.; Koh, K.; Tsujii, Y.; Fukuda, T. *Macromolecules* **2002**, *35*, 8989. (g) Pyun, J.; Jia, S.; Kowalewski, T.; Patterson, G. D.; Matyjaszewski, K. *Macromolecules* **2003**, *36*, 5094−5104. (h) Percy, M. J.; Michailidou, V.; Armes, S. P.; Perruchot, C.; Watts, J. F.; Greaves, S. J. *Langmuir* **2003**, *19*, 2072. (i) Mori, H.; Müller, A. H. E.; Klee, J. E. *J. Am. Chem. Soc.* **2003**, *125*, 3712. (j) Lui, T.; Jia, S.; Kowalewski, T.; Matyjaszewski, K. *Langmuir* **2003**, *19*, 6342. (k) Li, C.; Schmidt, M.; Chen, Y. *Polym. Prepr.* **2003**, *44*, 568.

(9) Lindner, P. In *Neutrons, X-ray and Light Scattering Methods Applied to Soft Condensed Matter*; Lindner, P., Zemb, T., Eds.; North-Holland Series; Elsevier: Amsterdam, 2002; Chapter 2, p 23.

(10) (a) Scriven, E. F. V. *Chem. Soc. Rev.* **1983**, *12*, 129. (b) Moore, J. S.; Stupp, S. I. *Macromolecules* **1990**, *23*, 65−70.

(11) Pedersen, J. S. In *Neutrons, X.-Ray and Light Scattering Methods Applied Soft Condensed Matter*; Lindner, P., Zemb, T., Eds.; North-Holland Series; Elsevier: Amsterdam, 2002; p 391.

MA035959W